Optical Generation and Distribution of Continuously Tunable Millimeter-Wave Signals Using an Optical Phase Modulator

Guohua Qi, Jianping Yao, *Senior Member, IEEE, Member, OSA*, Joe Seregelyi, Stéphane Paquet, and Claude Bélisle

***Abstract*—In this paper, we propose an approach to generate and distribute two wide bands of continuously tunable millimeter-wave (mm-wave) signals using an optical phase modulator and a fixed optical notch filter. We demonstrate theoretically that the odd-order electrical harmonics are cancelled and even-order electrical harmonics are generated at the output of a photodetector when the optical carrier is filtered out from the phase-modulated optical spectrum. Analysis shows that dispersion compensation is required in order to maintain the suppression of the odd-order electrical harmonics, in order to eliminate signal fading of the generated electrical signal when the optical signal is distributed using conventional single-mode optical fiber. It is experimentally demonstrated that, when the electrical drive signal is tuned from 18.8–25 GHz, two bands of mm-wave signals from 37.6 to 50 GHz and from 75.2 to 100 GHz with high signal quality are generated locally and remotely. This approach does not suffer from the direct current (dc) bias-drifting problem observed when an optical intensity modulator is used.**

***Index Terms*—Fiber Bragg grating (FBG), microwave photonics, millimeter-wave (mm-wave) generation, optical heterodyne, optical phase modulator.**

I. Introduction

OPTICALLY generated microwave and millimeter-wave (mm-wave) signals can find applications in many fiber-supported microwave and mm-wave systems, such as broadband wireless access networks, software-defined radio, antenna remoting, phased-array antenna, optical sensors, and radar systems [1]. These systems take advantage of the extremely low transmission loss (0.2 dB/km) of the standard single-mode fiber (SMF) and the availability of erbium-doped fiber amplifier (EDFA) at the 1550-nm band for distributing microwave and mm-wave signals over long distances.

These microwave and mm-wave signal sources have been extensively investigated with most work to date focusing on high-frequency electrical signal generation—especially on mm-wave signal generation up to the 60-GHz band with narrow-bandwidth optical components. This is because high-frequency electrical signal generation using conventional electronics becomes less financially attractive for systems operating above about 26 GHz, and their distribution via wireless or coaxial methods is highly challenging when compared with optical methods. On the other hand, low-frequency electrical carriers can be generated by direct modulation of a laser diode (LD) or by external modulation using an optical intensity modulator. When compared with high-frequency signals, the power penalty and phase-noise degradation induced on these low-frequency signals by chromatic dispersion of the fiber is less severe, even without dispersion compensation [2]–[4].

Many different approaches have been proposed to design mm-wave sources based on optical heterodyne techniques. They can be roughly classified into two types: one type is based on two stabilized lasers, and the other is based on one laser plus an external optical modulator. Methods based on two stabilized lasers include the use of injection locking [5] and phase-locked loops [6]. Methods with one laser plus an external optical modulator have shown great potential for producing high-purity mm-wave signals [7]–[9]. These approaches are based on the inherent nonlinearity of the phase modulator's response and, as a result, a high-frequency electrical signal can be optically generated with a low-frequency drive signal. Frequency doubling [7] or quadrupling [8], [9] becomes achievable. This dramatically lowers the bandwidth requirements for the optical modulator, the electrical drive signal source, and the drive circuit itself. For the frequency-quadrupling approaches [8], [9], additional components such as Mach–Zehnder interferometer-based [8] or Fabry–Pérot (FP) [9] filters are used to select the desired optical sidebands in order to obtain an electrical signal with a clean spectrum. The free spectral range (FSR) of these optical filters determines the frequency of the generated electrical signal. These methods work well for fixed-frequency applications, but for systems with frequency reconfigurability, such as wide-band surveillance radar, spread-spectrum, or software-defined radio, continuously tunable mm-wave signals are required.

Tunable optical filters would be required to realize a tunable mm-wave source using the methods mentioned in [8] and [9]. This adds extra complexity that can be avoided by exploring other approaches. The method described in [7] provides a solution to generate a tunable frequency-doubled electrical signal. The direct current (dc) bias is adjusted to suppress the even-order optical sidebands from the optical intensity-modulator

Manuscript received November 30, 2004; revised April 20, 2005. This work was supported by the Canadian Institute for Photonic Innovations.

G. Qi and J. Yao are with the Microwave Photonics Research Laboratory, School of Information Technology and Engineering, University of Ottawa, Ottawa, ON, Canada K1N 6N5 (e-mail: jpyao@site.uottawa.ca).

J. Seregelyi, S. Paquet, and C. Bélisle are with the Communications Research Centre, Ottawa, ON, Canada K2H 8S2.

Digital Object Identifier 10.1109/JLT.2005.854067

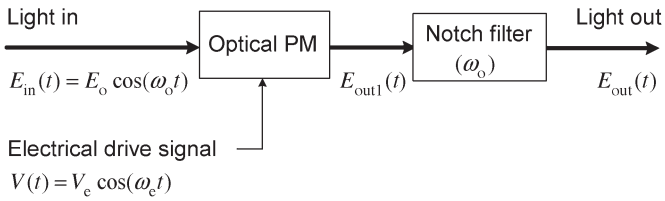

Fig. 1. Schematic diagram of the proposed mm-wave generation method (Optical PM: optical phase modulator).

output spectrum. Therefore, an optical filter is not needed. However, biasing the intensity modulator to suppress the even-order optical sidebands suffers from a dc bias-drifting problem, which reduces the robustness of the system.

In this paper, we propose a robust method for the optical generation of two bands of continuously tunable mm-wave signals using an optical phase modulator and a fixed optical notch filter. Frequency doubling and quadrupling of the electrical drive signal can be achieved without specific dc bias adjustment. A theoretical model of the proposed method and a mathematical analysis of the chromatic dispersion effect on the generated signal when distributed over optical fiber are presented. We successfully generate two bands of mm-wave signals that can be tuned from 37.6 to 50 GHz with frequency doubling, and from 75.2 to 100 GHz with frequency quadrupling, using a commercially available optical phase modulator and a fiber Bragg grating (FBG) serving as the fixed optical notch filter. We show that the quality of the signal remains unchanged when remote generation is performed at the end of a 60-km span of SMF with proper dispersion compensation.

II. Analysis

A. Principle of the Proposed Approach

A well-known method for optical generation of electrical signals is based on the optical heterodyne technique. In our proposed approach, the two optical carriers used for heterodyning originate from the same optical source. As a result, there is a high level of phase-noise correlation between the two carriers. Therefore, the generated signal will have low phase noise and stable amplitude and frequency, a requirement for most system applications.

The operating principle of the proposed method is illustrated in Fig. 1. To simplify the analysis, we use pure sinusoidal signals to represent the electrical and optical sources without loss of generality. The waveform at the output of an optical phase modulator $E_{\mathrm{out1}}(t)$ driven by a pure sinusoidal electrical signal is given by

$$E_{\mathrm{out1}}(t) = E_{\mathrm{o}} \sum_{n=-\infty}^{\infty} J_n(\beta) \cos\left[(\omega_{\mathrm{o}} + n\omega_{\mathrm{e}})t + n \cdot \frac{\pi}{2}\right] \quad (1)$$

where E_{o} and ω_{o} are the amplitude and angular frequency of the optical carrier; ω_{e} is the angular frequency of the electrical drive signal; and $J_n(\beta)$ is a Bessel function of the first kind of order n with argument of β. $\beta = (\pi/V_\pi) \cdot V_{\mathrm{e}}$ is related to the phase-modulation depth, where V_π is the half-wave voltage of the optical phase modulator and V_{e} is the amplitude of the electrical drive signal.

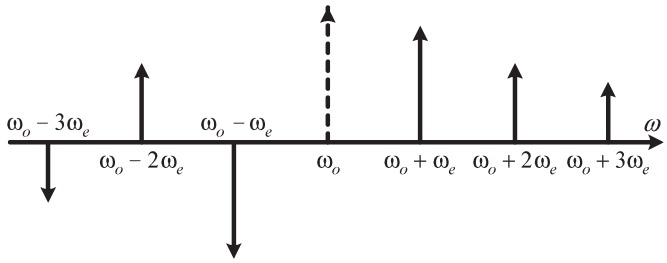

Fig. 2. Optical spectrum at the output of the notch filter (the dashed line shows the removed optical carrier by the notch filter).

Equation (1) shows that the power of the input optical carrier will be spread out to the first-, second-, third- and higher order optical sidebands. The amplitude distribution of the sidebands is governed by the variation of the Bessel functions parameterized by β. Although (1) indicates that there are many optical sidebands at the output of the phase modulator, their beating at a photodetector will only generate a dc component. This is because all of the optical sidebands are related in amplitude and phase, and as a result, the beat products cancel. This behavior is expected since the phase modulation does not alter the amplitude of the input optical carrier, and the square-law photodetector works like an envelope detector. Once converted to the electrical domain, the unfiltered optical output of the phase modulator can be mathematically expressed as

$$\begin{aligned} V_{\mathrm{out1}}(t) &= C\left[\sum_{n=-\infty}^{\infty} J_n(\beta)\cos\left[(\omega_{\mathrm{o}} + n\omega_{\mathrm{e}})t + n\cdot\frac{\pi}{2}\right]\right]^2 \\ &= \frac{C}{2}\sum_{n=-\infty}^{\infty}[J_n(\beta)]^2 = \frac{C}{2} \end{aligned} \quad (2)$$

where C is a constant, which is related to E_{o} and the responsivity of the photodetector. The intrinsic insensitivity of the photodetector to the phase of the optical carrier means that only the amplitude is detected, and the dc component at its output will be proportional to that amplitude. Note that, in (2), all terms proportional to $\cos[2(\omega_{\mathrm{o}} + n\omega_{\mathrm{e}})t + n\pi]$, $(n = -\infty, +\infty)$ are omitted because of the limited bandwidth of the receiving circuit.

Next, we filter out the optical carrier at the output of the phase modulator using a notch filter. The electric field at the output of the filter can be expressed as

$$\begin{aligned} &E_{\mathrm{out}}(t) \\ &= E_{\mathrm{o}}\left\{\sum_{n=-\infty}^{\infty} J_n(\beta)\cos\left[(\omega_{\mathrm{o}}+n\omega_{\mathrm{e}})t+n\cdot\frac{\pi}{2}\right] - J_0(\beta)\cos(\omega_{\mathrm{o}}t)\right\}. \end{aligned} \quad (3)$$

The spectrum at the output of the notch filter consists of a series of impulses, each with their own amplitude and phase. An example of such a spectrum is shown in Fig. 2. Here, the additional $\pi/2$ phase shift between each impulse is not shown. The dashed line represents the optical carrier removed by the notch filter.

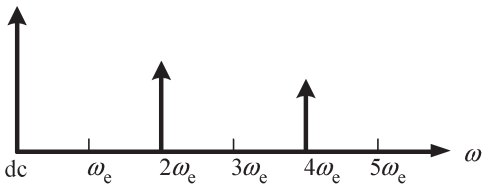

Fig. 3. Electrical spectrum at the output of a photodetector.

When these optical sidebands are fed to a photodetector, high-frequency electrical signals are generated. The voltage expression of the generated electrical signals $V_{\text{out}}(t)$ is

$$\begin{aligned} V_{\text{out}}(t) &= C\Bigg\{ \left[\sum_{n=-\infty}^{\infty} J_n(\beta) \cos\left[(\omega_o + n\omega_e)t + n \cdot \frac{\pi}{2} \right] \right]^2 \\ &\quad + [J_0(\beta)\cos(\omega_o t)]^2 - 2 \sum_{n=-\infty}^{\infty} J_n(\beta) \\ &\quad \cdot J_0(\beta) \cos\left[(\omega_o + n\omega_e)t + n \cdot \frac{\pi}{2} \right] \cdot \cos(\omega_o t) \Bigg\} \\ &= C\left\{ \frac{1}{2} + \frac{1}{2} \cdot [J_0(\beta)]^2 - \sum_{n=-\infty}^{\infty} J_n(\beta) \right. \\ &\quad \left. \cdot J_0(\beta) \cos\left[n\left(\omega_e t + \frac{\pi}{2} \right) \right] \right\} \\ &= C\left\{ \frac{1}{2} - \frac{1}{2} \cdot [J_0(\beta)]^2 - 2\sum_{n=1}^{\infty} J_{2n}(\beta) \right. \\ &\quad \left. \cdot J_0(\beta) \cos\left[2n\left(\omega_e t + \frac{\pi}{2} \right) \right] \right\}. \end{aligned} \tag{4}$$

Here, the property of the Bessel function $J_{-n}(\beta) = (-1)^n J_n(\beta)$ is used and the limited bandwidth of the receiving circuit is also taken into consideration.

In (4), the first two terms $C/2$ and $-(C/2) \cdot [J_0(\beta)]^2$ are dc components. The third term, $-2C \sum_{n=1}^{\infty} J_{2n}(\beta) \cdot J_0(\beta) \cos[2n(\omega_e t + (\pi/2))]$, represents an infinite number of even-order electrical harmonics of the electrical drive signal with the peak magnitude of each harmonic decaying according to the Bessel function distribution. Equation (4) clearly indicates that there are no odd-order harmonic terms in the optically generated electrical signals once the carrier is removed. This mathematically demonstrates that the proposed configuration is able to generate optically even-order harmonics of the electrical drive signal and suppress all odd-order harmonics.

By adjusting V_e, the modulation depth β is set such that the optical sidebands up to the fourth order dominate the optical power. As a result, the second- and fourth-order electrical harmonics will be generated, and higher order harmonics can then be ignored. The spectrum of the generated electrical signal is illustrated in Fig. 3.

For maximizing the power of the generated second- and fourth-order electrical harmonics, β can be adjusted in (4) to get the maximum value of $J_2(\beta) \cdot J_0(\beta)$ and $J_4(\beta) \cdot J_0(\beta)$.

Our signal-generation scheme provides the possibility of generating tunable electrical signals by tuning the frequency of the electrical drive signal without changing the optical carrier frequency. Then, a notch filter, with a fixed central wavelength, can be employed to remove the carrier. For example, if the optical phase modulator is driven by an 8–16-GHz signal, two bands of electrical signals with frequency of 16–32 GHz and 32–64 GHz can be obtained.

B. Transmission-Effect Analysis

A significant advantage of the optical generation of high-frequency electrical signals is the ease by which they can be distributed using optical fiber, without significant loss, over much greater distance than by using conventional electrical cables or waveguides. However, for propagation over many tens of kilometers of standard SMF, fiber attenuation, chromatic dispersion, and random polarization disturbances can affect the quality of the generated signal. The fiber attenuation can be easily compensated for with the use of EDFAs. Random polarization disturbances do not affect signals generated by optical heterodyne as much as in optical coherent communication systems, where the polarization state of the local optical carrier needs to track the polarization state of the incoming signal. In our optical heterodyne-based systems, the optical carrier and sidebands used for creating the electrical carrier are sent together. As a result, it is most likely that the polarization states of all the optical-signal components will change in a similar way as they propagate in the fiber.

Although the chromatic dispersion of the standard SMF is low $[D = 17\ \text{ps}/(\text{nm} \cdot \text{km})]$, it has to be considered when analyzing the quality of an electrical signal generated with our technique after the optical sidebands have traveled in a long fiber span. One key aspect is that odd-order electrical harmonics still have to be cancelled. To maintain the cancellation, the optical sidebands at the remote site must conserve the same amplitude and phase relations that existed at the beginning of the span. Cumulative effects from fiber chromatic dispersion will alter these relations, eventually resulting in a poor cancellation of the first- and third-order electrical harmonics, and in some, power penalty for the second- and fourth-order ones. We will now analyze the impact of chromatic dispersion on the resulting signal. Then, we will show that dispersion compensation will eliminate these detrimental effects on the generated electrical carrier.

1) Dispersion Effect: When fiber chromatic dispersion is taken into consideration, the propagation constant $\beta(\omega)$ of the fiber for an optical sideband at $\omega_o \pm n\omega_e$ can be approximately represented by a Taylor series around the center angular frequency ω_o [10]

$$\begin{aligned} \beta(\omega_o \pm n\omega_e) &= \beta(\omega_o) + \beta'(\omega_o)(\pm n\omega_e) \\ &\quad + \frac{1}{2}\beta''(\omega_o)(\pm n\omega_e)^2 + \ldots \end{aligned} \tag{5}$$

where the effect of higher order dispersion is neglected [11].

We can now give the mathematical representation of the first-order electrical harmonic $V_{\text{out,e1}}$ after the optical signal has

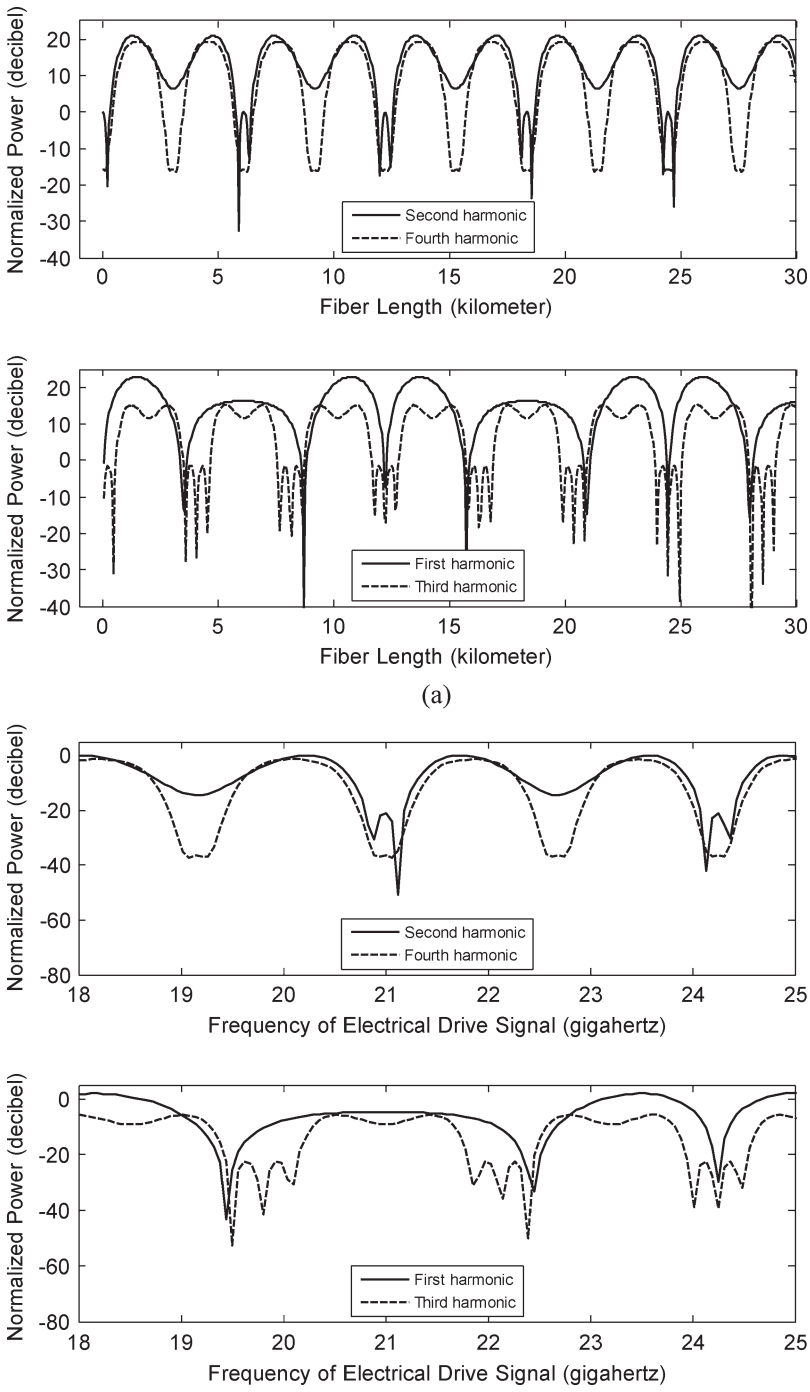

Fig. 4. Effects of the chromatic dispersion on the normalized power of generated electrical harmonics. (a) Normalized power versus fiber length. (b) Normalized power versus the frequency of the electrical drive signal.

traveled through a fiber span of length L. After electrooptical conversion, we have

$$V_{\mathrm{out,e1}}(t) = 2C\sum_{n=1}^{\infty} J_n(\beta)J_{n+1}(\beta) \times \sin\left[\frac{\beta''(\omega_{\mathrm{o}})}{2}(2n+1)\omega_{\mathrm{e}}^2 L\right]\sin\left[\omega_{\mathrm{e}}t + \frac{\pi}{2} - \beta'(\omega_{\mathrm{o}})\omega_{\mathrm{e}}L\right] \quad (6)$$

where $\sum_{n=-1}^{-\infty} J_n(\beta)J_{n-1}(\beta) = -\sum_{n=1}^{\infty} J_n(\beta)J_{n+1}(\beta)$ is used. The widely used chromatic-dispersion parameter D is related to $\beta''(\omega_{\mathrm{o}})$ by

$$D = -\frac{2\pi c}{\lambda_{\mathrm{o}}^2}\beta''(\omega_{\mathrm{o}}) \quad (7)$$

where c is the speed of light in free space, and λ_{o} is the wavelength of the optical carrier. Therefore, (6) can be expressed

in terms of D

$$V_{\mathrm{out,e1}}(t) = C\left\{-2\sum_{n=1}^{\infty} J_n(\beta)J_{n+1}(\beta)\sin\left[(2n+1)\pi LcD\left(\frac{f_\mathrm{e}}{f_\mathrm{o}}\right)^2\right]\right\} \times \cos\left[\omega_\mathrm{e}t - \beta'(\omega_\mathrm{o})\omega_\mathrm{e}L\right] \quad (8)$$

where f_e is the frequency of the electrical drive signal. Similarly, the second-order electrical harmonic $V_{\mathrm{out,e2}}$ can be expressed as

$$V_{\mathrm{out,e2}}(t) = C\left\{J_1^2(\beta) - 2\sum_{n=1}^{\infty} J_n(\beta)J_{n+2}(\beta) \times \cos\left[2(2n+2)\pi LcD\left(\frac{f_\mathrm{e}}{f_\mathrm{o}}\right)^2\right]\right\} \times \cos\left[2\omega_\mathrm{e}t - 2\beta'(\omega_\mathrm{o})\omega_\mathrm{e}L\right] \quad (9)$$

where $\sum_{n=-1}^{-\infty} J_n(\beta)J_{n-2}(\beta) = \sum_{n=1}^{\infty} J_n(\beta)J_{n+2}(\beta)$ is used. The third- and the fourth-order electrical harmonics $V_{\mathrm{out,e3}}$ and $V_{\mathrm{out,e4}}$ are

$$V_{\mathrm{out,e3}}(t) = C\left\{2\sum_{n=1}^{\infty} J_n(\beta)J_{n+3}(\beta) \times \sin\left[3(2n+3)\pi LcD\left(\frac{f_\mathrm{e}}{f_\mathrm{o}}\right)^2\right] - J_1(\beta)J_2(\beta)\sin\left[3\pi LcD\left(\frac{f_\mathrm{e}}{f_\mathrm{o}}\right)^2\right]\right\} \times \cos\left[3\omega_\mathrm{e}t - 3\beta'(\omega_\mathrm{o})\omega_\mathrm{e}L\right] \quad (10)$$

$$V_{\mathrm{out,e4}}(t) = C\left\{J_2^2(\beta) + 2\sum_{n=1}^{\infty} J_n(\beta)J_{n+4}(\beta) \times \cos\left[4(2n+4)\pi LcD\left(\frac{f_\mathrm{e}}{f_\mathrm{o}}\right)^2\right] - 2J_1(\beta)J_3(\beta)\cos\left[8\pi LcD\left(\frac{f_\mathrm{e}}{f_\mathrm{o}}\right)^2\right]\right\} \times \cos\left[4\omega_\mathrm{e}t - 4\beta'(\omega_\mathrm{o})\omega_\mathrm{e}L\right]. \quad (11)$$

Equations (8)–(11) show that the amplitudes of the first four electrical harmonics are determined by the value of $LcD(f_\mathrm{e}/f_\mathrm{o})^2$. The level of cancellation of the odd-order electrical harmonics and the power penalty on the even-order harmonics at the other end of the fiber span depends on D and f_e. Hence, as the signal frequency is tuned, the cancellation and power penalty level will change. Obviously, this is not a desirable effect. To overcome these problems, dispersion compensation is required. The variation of the power in the four harmonics calculated using (8)–(11) is shown in Fig. 4. The power variation is plotted as a function of the fiber length [Fig. 4(a)] and the frequency of the electrical signal that drives the modulator [Fig. 4(b)]. In Fig. 4(a), all values are normalized to the power of the second harmonic when the fiber length is zero (local detection). The other parameters used in Fig. 4(a) are set as follows: $D = 17\ \mathrm{ps/(nm \cdot km)}$, $\beta = 2.5$, $f_\mathrm{o} = 1550\ \mathrm{nm}$, $c = 3 \times 10^8\ \mathrm{m/s}$, and $f_\mathrm{e} = 24.5\ \mathrm{GHz}$. In Fig. 4(b), all values are normalized to the power of the second harmonic when the frequency of the electrical drive signal is 18 GHz. All the parameters are the same in Fig. 4(b), except for L, which is fixed at 25 km, and f_e, which is varied between 18 and 25 GHz.

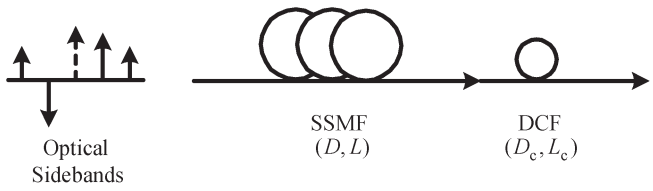

Fig. 5. Dispersion compensation using DCF for optical distribution of mm-wave signal (SSMF: standard single-mode fiber; DCF: dispersion-compensating fiber).

2) With Dispersion Compensation: One way to compensate for fiber dispersion is to insert a length of dispersion-compensating fiber (DCF) at the end of the span. Fig. 5 shows the dispersion-compensation arrangement. A DCF of chromatic dispersion parameter D_c and length L_c is connected after the transmission fiber, as shown in Fig. 5.

The DCF will compensate for the phase shifts that are induced on the optical sidebands while they are traveling in the fiber span, bringing them back in phase as much as possible. Now, the phase delay $\Phi(\omega)$ of each of these optical sidebands is expressed in terms of the propagation constant and fiber length of both the standard fiber and the DCF, respectively.

$$\Phi(\omega) = \beta(\omega)L + \beta_\mathrm{c}(\omega)L_\mathrm{c} \quad (12)$$

where $\beta_\mathrm{c}(\omega)$ is the propagation constant of the DCF. With the same analysis process as above, the expressions of the generated electrical signals at a photodetector can be obtained, as follows:

$$V_{\mathrm{out,e1c}}(t) = C\left\{-2\sum_{n=1}^{\infty} J_n(\beta)J_{n+1}(\beta) \times \sin\left[(2n+1)\pi c(LD + L_\mathrm{c}D_\mathrm{c})\left(\frac{f_\mathrm{e}}{f_\mathrm{o}}\right)^2\right]\right\} \times \cos\left\{\omega_\mathrm{e}t - \omega_\mathrm{e}\left[\beta'(\omega_\mathrm{o})L + \beta_\mathrm{c}'(\omega_\mathrm{o})L_\mathrm{c}\right]\right\} \quad (13)$$

$$V_{\mathrm{out,e2c}}(t) = C\left\{J_1^2(\beta) - 2\sum_{n=1}^{\infty} J_n(\beta)J_{n+2}(\beta) \times \cos\left[2(2n+2)\pi c(LD + L_\mathrm{c}D_\mathrm{c})\left(\frac{f_\mathrm{e}}{f_\mathrm{o}}\right)^2\right]\right\} \times \cos\left\{2\omega_\mathrm{e}t - 2\omega_\mathrm{e}\left[\beta'(\omega_\mathrm{o})L + \beta_\mathrm{c}'(\omega_\mathrm{o})L_\mathrm{c}\right]\right\} \quad (14)$$

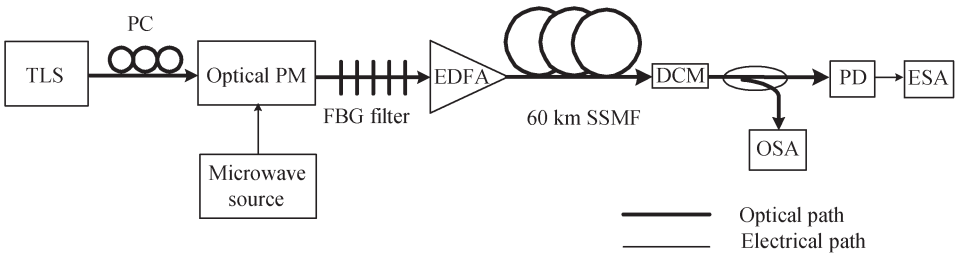

Fig. 6. Experimental setup for optical generation of mm-wave signals (TLS: tunable laser source; PC: polarization controller; Optical PM: optical phase modulator; EDFA: erbium-doped fiber amplifier; SSMF: standard single-mode fiber; DCM: dispersion-compensation module; OSA: optical spectrum analyzer; PD: photodetector; and ESA: electrical spectrum analyzer).

$$V_{\mathrm{out,e3c}}(t) = C\left\{2\sum_{n=1}^{\infty} J_n(\beta)J_{n+3}(\beta) \times \sin\left[3(2n+3)\pi c(LD+L_{\mathrm{c}}D_{\mathrm{c}})\left(\frac{f_{\mathrm{e}}}{f_{\mathrm{o}}}\right)^2\right] - J_1(\beta)J_2(\beta)\sin\left[3\pi c(LD+L_{\mathrm{c}}D_{\mathrm{c}})\left(\frac{f_{\mathrm{e}}}{f_{\mathrm{o}}}\right)^2\right]\right\} \times \cos\left\{3\omega_{\mathrm{e}}t - 3\omega_{\mathrm{e}}\left[\beta'(\omega_{\mathrm{o}})L + \beta'_{\mathrm{c}}(\omega_{\mathrm{o}})L_{\mathrm{c}}\right]\right\} \quad (15)$$

$$V_{\mathrm{out,e4c}}(t) = C\left\{J_2^2(\beta) + 2\sum_{n=1}^{\infty} J_n(\beta)J_{n+4}(\beta) \times \cos\left[4(2n+4)\pi c(LD+L_{\mathrm{c}}D_{\mathrm{c}})\left(\frac{f_{\mathrm{e}}}{f_{\mathrm{o}}}\right)^2\right] - 2J_1(\beta)J_3(\beta)\cos\left[8\pi c(LD+L_{\mathrm{c}}D_{\mathrm{c}})\left(\frac{f_{\mathrm{e}}}{f_{\mathrm{o}}}\right)^2\right]\right\} \times \cos\left\{4\omega_{\mathrm{e}}t - 4\omega_{\mathrm{e}}\left[\beta'(\omega_{\mathrm{o}})L + \beta'_{\mathrm{c}}(\omega_{\mathrm{o}})L_{\mathrm{c}}\right]\right\} \quad (16)$$

where $V_{\mathrm{out,e1c}}(t)$, $V_{\mathrm{out,e2c}}(t)$, $V_{\mathrm{out,e3c}}(t)$, and $V_{\mathrm{out,e4c}}(t)$ are the generated electrical signals at the end of the DCF. When $LD + L_{\mathrm{c}}D_{\mathrm{c}} = 0$, it is clear that $V_{\mathrm{out,e1c}}(t)$ and $V_{\mathrm{out,e3c}}(t)$ are equal to zero, as can be seen in (13) and (15); $V_{\mathrm{out,e2c}}(t)$ and $V_{\mathrm{out,e4c}}(t)$ reach their respective maximum value. When the dispersion parameter of the DCF D_{c} is given, the required length L_{c} for proper compensation is calculated by

$$L_{\mathrm{c}} = -\frac{D}{D_{\mathrm{c}}}L. \quad (17)$$

III. Experiment

The experimental setup used to verify the performance of the proposed signal-generation method is illustrated in Fig. 6.

The optical phase modulator is a commercially available 1550-nm $LiNbO_3$ modulator. A tunable laser is used as the optical source. The optical carrier generated by the tunable laser source (TLS) is sent to the phase modulator through a polarization controller (PC). The wavelength of the optical carrier is set to match the maximum attenuation wavelength of the FBG notch filter. A microwave-signal source tunable from 12.5 to 25 GHz is applied to the phase modulator. Optical sidebands at the output of the FBG filter are amplified with an EDFA and then transmitted over 60 km of standard SMF. The beating of these optical sidebands at a photodetector generates the required mm-wave signals.

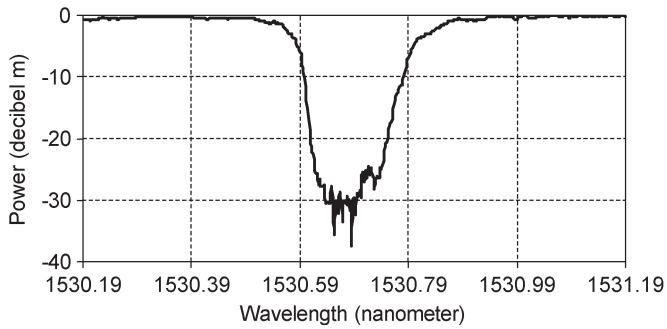

Fig. 7. Transmission spectrum of the FBG filter.

The transmission spectrum of the FBG notch filter is shown in Fig. 7. The bandwidth from the minimum attenuation point at lower wavelengths to the minimum attenuation point at longer wavelengths is about 0.3 nm ($\approx$ 37.5 GHz).

Measurements have been taken before and after transmission, with and without dispersion compensation, in order to analyze and evaluate the performance of the system. Fig. 8 shows the typical optical spectra before and after the FBG filter. Here, the optical phase modulator is driven by a 12.5-GHz signal. Fig. 8(a) shows that optical sidebands are generated up to the fourth order. They are distributed symmetrically around the optical carrier. Fig. 8(b) shows the optical spectrum after the FBG filter. It is clearly shown that the optical carrier power is attenuated to about 40 dB. Due to the bandwidth of the FBG and its asymmetric attenuation characteristics, the first-order optical sidebands are not attenuated to the same level on each side of the carrier. This is an issue for drive frequencies up to about 19 GHz for this particular FBG, but the problem can be avoided by operating at higher frequencies or, in the future, by improving the spectrum symmetry of the FBG.

Fig. 9 shows the spectrum of the optically generated electrical signal, measured at the output of the photodetector before transmission. The spectrum corresponds to a 24.5-GHz electrical drive signal—a frequency where the first-order optical harmonics are not attenuated by the FBG. It is easily seen that an mm-wave signal at twice the frequency of the drive electrical signal is generated. Signal components above 50 GHz

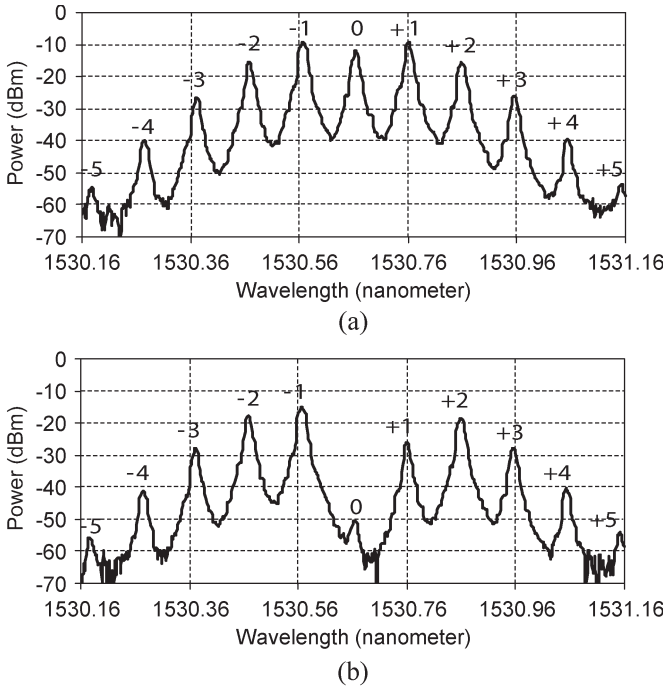

Fig. 8. Typical optical spectra before transmission (+, −: optical sideband in upper frequency side and lower frequency side; 0: optical carrier; and 1, 2, 3, 4, 5: first-, second-, third-, fourth-, and fifth-order optical sideband). (a) Before the FBG filter. (b) After the FBG filter.

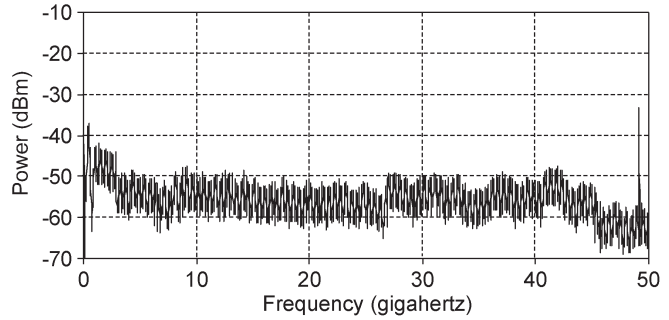

Fig. 9. Electrical spectrum of the generated mm-wave signals when the drive signal frequency is 24.5 GHz.

are not visible due to the bandwidth limit of the photodetector and the electrical spectrum analyzer; however, they are present in the output when viewed on the optical spectrum analyzer (OSA). When the electrical drive signal is tuned from 18.8 to 25 GHz, two bands of mm-wave signals from 37.6 to 50 GHz and from 75.2 to 100 GHz with high frequency stability and narrow linewidth are generated. These observations agree well with the outcome of the mathematical analysis presented in the previous section.

As can be seen in Fig. 7, the attenuation of the FBG filter on its lower and upper frequency slopes is not symmetrical with respect to the center of the notch. As such, the group delay is also not symmetrical. If the sidebands of the modulated optical signal fall in this section of the filter bandwidth, the nonsymmetrical characteristic will break down the intrinsic amplitude and phase relationship among the optical sidebands of a phase modulated signal. The power of the required

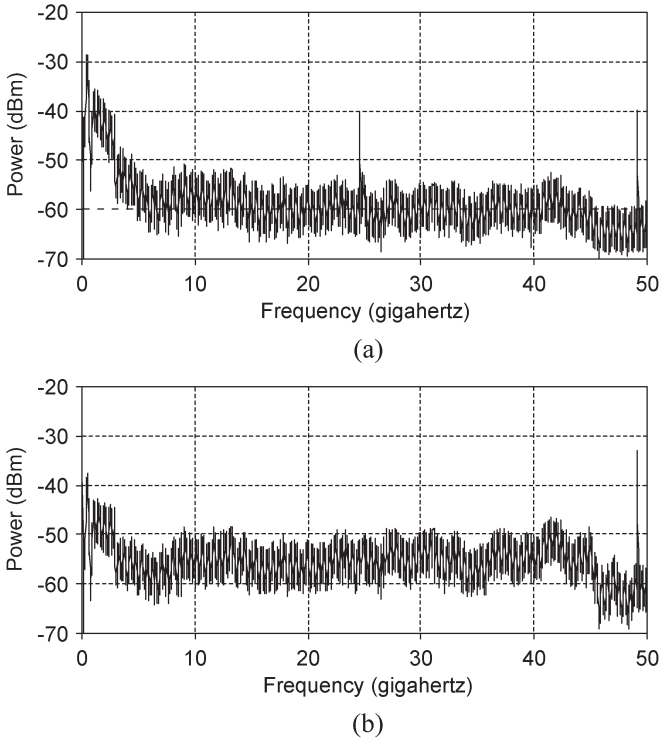

Fig. 10. Electrical spectra of the generated mm-wave signals after transmission over a 60-km standard single-mode fiber. (a) Without dispersion-compensation module. (b) With dispersion-compensation module.

mm-wave signal and the odd-order harmonic suppression will be affected. To avoid this, the electrical drive signal must have a low-frequency criterion. The lowest frequency of the electrical drive signal should be equal to or greater than half of the frequency bandwidth of the FBG. In this case, the generated mm-wave signal is only affected by the maximum attenuation at the center of the notch, and it is immunized from the imperfect characteristics of the FBG, including its large dispersion effect.

Fig. 10 shows the electrical spectra of the remotely generated electrical signals when the electrical drive signal is at 24.5 GHz, after propagation over a 60-km SMF. Fig. 10(a) is an indication of the spectrum without dispersion compensation, while Fig. 10(b) is the spectrum when dispersion compensation is applied before photodetection. In Fig. 10(a), the 24.5-GHz signal is not fully cancelled, and the amplitude of the 49-GHz signal decreases due to a chromatic-dispersion-induced power penalty. Fig. 10(b) clearly shows the cancellation of the 24.5-GHz signal and the elimination of the power penalty to the 49-GHz signal when chromatic dispersion compensation is used. These measurements are in accordance with the analysis conclusion presented in Section II-B.

Fig. 11 gives zoom-in views of the electrical spectra of the optically generated 49-GHz electrical signal before and after transmission with dispersion compensation. The resolution bandwidth of the electrical spectrum analyzer is 1 and 100 Hz in Fig. 11(a) and (b), respectively. It can be seen that the 49-GHz electrical signal does not suffer from obvious phase-noise degradation after the 60-km transmission. The quality of the signal is adequate for most practical applications.

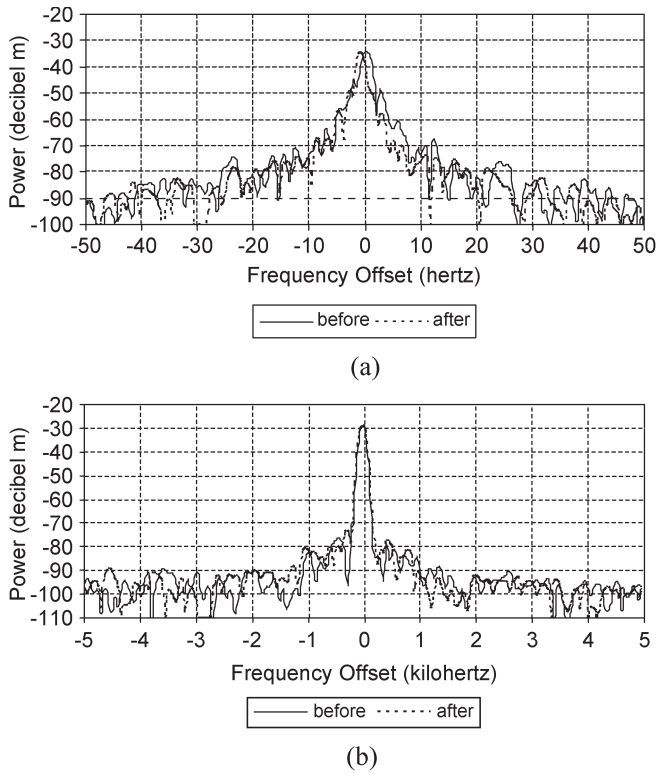

Fig. 11. Electrical spectra of the signal generated before and after transmission with dispersion compensation. (a) Span 100 Hz. (b) Span 10 kHz.

IV. Conclusion

We have proposed a new and robust method for the optical generation of wideband continuously tunable millimeter-wave (mm-wave) signals. The mathematical foundations of the method have been detailed, and an experimental verification of its performance has been performed. In the proposed configuration, an optical phase modulator and a fiber Bragg grating (FBG) notch filter were used. The optical carrier was removed from the output of the optical phase modulator by the FBG notch filter. When the resulting optical sidebands were applied to a photodetector, only even-order electrical harmonics were generated, and the odd-order harmonics were cancelled. The effect of chromatic dispersion in the fiber used to distribute the signal on the generated electrical signal was also analyzed.

Experimental validation with an electrical drive signal tuned from 18.8 to 25 GHz has been conducted. Two bands of mm-wave signals from 37.6 to 50 GHz and 75.2 to 100 GHz (signal components above 50 GHz are only visible on the OSA) were generated locally and remotely. The generated signals had high-frequency stability and narrow linewidth. It was verified that, after dispersion compensation, the integrity of the generated signals was maintained after transmission over a 60-km SMF.

A major advantage of the proposed approach is that continuously tunable mm-wave signals over a wide frequency range can be generated using a fixed optical filter, which significantly simplifies the system configuration. Compared with the approaches based on an optical intensity modulator, the phase modulator does not need a direct current (dc) bias, thus eliminating dc bias-drifting related problems.

Acknowledgment

The authors would like to thank J. Oldham and D. Barlow of the communications Research Centre Canada, and F. Zeng and X. Chen of the University of Ottawa for their assistance in the experiments.

References

[1] R. P. Braun, G. Grosskopf, D. Rohde, and F. Schmidt, "Optical millimetre-wave generation and transmission experiments for mobile 60 GHz band communications," *Electron. Lett.*, vol. 32, no. 7, pp. 626–628, Mar. 28, 1996.

[2] H. Schmuck, "Comparison of optical millimeter-wave system concepts with regard to chromatic dispersion," *Electron. Lett.*, vol. 31, no. 21, pp. 1848–1849, Oct. 12, 1995.

[3] U. Gliese, S. Norskov, and T. N. Nielsen, "Chromatic dispersion in fiber-optic microwave and millimeter-wave links," *IEEE Trans. Microw. Theory Tech.*, vol. 44, no. 10, pp. 1716–1724, Oct. 1996.

[4] G. Qi, J. Yao, J. Seregelyi, S. Paquet, and J. C. Bélisle, "Phase noise analysis of the optically generated and distributed millimeter wave signal using an external optical modulator," in *Photonics North*, Montreal, QC, Canada, Sep. 2004, vol. 5579C, pp. 598–606.

[5] L. Goldberg, H. F. Taylor, J. F. Weller, and D. M. Bloom, "Microwave signal generation with injection-locked laser diodes," *Electron. Lett.*, vol. 19, no. 13, pp. 491–493, Jun. 23, 1983.

[6] R. T. Ramos and A. J. Seeds, "Fast heterodyne optical phase lock loop using double quantum well laser diodes," *Electron. Lett.*, vol. 28, no. 1, pp. 82–83, Jan. 2, 1992.

[7] J. J. O'Reilly, P. M. Lane, R. Heidemann, and R. Hofstetter, "Optical generation of very narrow linewidth millimetre wave signals," *Electron. Lett.*, vol. 28, no. 25, pp. 2309–2311, Dec. 3, 1992.

[8] J. J. O'Reilly and P. M. Lane, "Fibre-supported optical generation and delivery of 60 GHz signals," *Electron. Lett.*, vol. 30, no. 16, pp. 1329–1330, Aug. 4, 1994.

[9] P. Shen, N. J. Gomes, P. A. Davies, W. P. Shillue, P. G. Huggard, and B. N. Ellison, "High-purity millimetre-wave photonic local oscillator generation and delivery," in *Proc. Int. Topical Meeting Microwave Photonics*, Budapest, Hungary, Sep. 10–12, 2003, pp. 189–192.

[10] K. Okamoto, *Fundamentals of Optical Waveguides*. New York: Academic, 2000, p. 72.

[11] W. K. Marshall, B. Crosignani, and A. Yariv, "Laser phase noise to intensity noise conversion by lowest-order group-velocity dispersion in optical fiber: Exact theory," *Opt. Lett.*, vol. 25, no. 3, pp. 165–167, 2000.

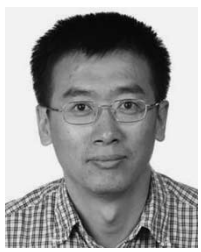

Guohua Qi received the B.E. and M.S. degrees in electrical engineering from Beijing University of Posts and Telecommunications, Beijing, China, in 1986 and 1989, respectively. He is currently working toward the Ph.D. degree at the School of Information Technology and Engineering, University of Ottawa, Ottawa, ON, Canada.

He joined Nanjing Electronic Devices Institute (NEDI), Nanjing, China, in 1989, where he was engaged in the research and development of microwave solid-state circuits, modules, and subsystems for the next twelve years. His current research interests include microwave photonics, radio-over-fiber, and software-defined radio.

Jianping Yao (M'99–SM'01) received the Ph.D. degree in electrical engineering from the University of Toulon, Toulon, France, in 1997.

From January 1998 to July 1999, he was a Research Fellow, and from July 1999 to December 2001, he was an Assistant Professor, both with the School of Electrical and Electronic Engineering, Nanyang Technological University, Singapore. He was an Invited Professor in the Institut National Polytechnique de Grenoble, Grenoble, France, from January to March 2005. He has published over 100 papers in refereed journals and conference proceedings. His current research interests include optical signal processing, optically controlled phased-array antennas, photonic generation of microwave signals, radio-over-fiber systems, fiber lasers and amplifiers, broadband infrared wireless home networking, and fiber-optic sensors. He is an Associate Professor in the School of Information Technology and Engineering, University of Ottawa, Ottawa, ON, Canada.

Dr. Yao is a Member of the International Society for Optical Engineers (SPIE) and the Optical Society of America (OSA).

Joe Seregelyi received the M. Eng. degree in engineering physics from McMaster University, Hamilton, ON, Canada, in 1987.

He joined the National Research Council in 1988 and worked in the area of pulsed electromagnetics. He has been at the Communications Research Centre, Ottawa, ON, Canada since 1993, and is currently Research Engineering/Project Leader in microwave-photonics. He has extensive knowledge in the areas of radio frequency (RF) and microwave design (signal integrity, circuit design, electromagnetic compatibility, antenna design, high-power microwaves (HPM), and ultra-wideband radar and communications). He also has been doing optical design work for a number of years [high-power lasers, antenna remoting, communications systems and infrared (IR) imaging]. He has published over 50 technical papers and reports and holds patents in the area of hybrid IR/HPM landmine detection and neutralization.

Stéphane Paquet received the M.Sc. degree in optics from Laval University, QC, Canada, in 1993.

He joined the National Optics Institute, QC, Canada, working on the design and fabrication of integrated optics components. Later, he moved to MPB Technologies, Montreal, QC, Canada, as part of the space-technology and optical-amplifier research and development groups. In 1997, he pursued his career at Nortel Networks, where he initially became part of the Communication-Systems Engineering Group in Montreal, QC, Canada. Later, he continued as an Optical System Designer in Ottawa, ON, Canada, and as a Researcher in the Optical Components R&D Group in Harlow, U.K. Currently, he works at Communications Research Centre, Ottawa, ON, Canada, in the microwave photonic research field.

Claude Bélisle received the Bachelor's degree in engineering physics from the Royal Military College of Canada, Kingston, ON, Canada, and the Master's degree in physics-optics from Laval University, QC, Canada.

He has been involved in various research and development projects related to satellite communications for both military and commercial applications at DRDC–Ottawa, Ottawa, ON, Canada, and the Communications Research Centre (CRC), Ottawa, ON, Canada, for close to 20 years. He is currently the Research Manager of the CRC Advanced Radio System Group, where he leads research in microwave-photonics technologies, satellite communications networks, and software-defined radio. He is also a Director of the Software-Defined Radio Forum.